Chapter 16

Constructing a Magnetic Tweezers to Monitor RNA Translocation at the Single-Molecule Level

Desiree Salas, Veronika Gocheva, and Marcelo Nöllmann

Abstract

Single-molecule methods have become an invaluable tool in the investigation of the mechanisms of nucleic-acid motors. Magnetic tweezers is a single-molecule manipulation technique that permits the real-time measurement of enzyme activities on single nucleic-acid molecules at high-resolution, high-throughput, and inherently constant force. Here, we describe several aspects of the implementation of magnetic tweezers, with special emphasis on the construction of a simple magnetic trap and, in particular, on the detailed description of image analysis methods to measure the extension changes in nucleic-acid molecules induced by protein activity. Finally, we carefully describe the steps involved in performing a full magnetic tweezers experiment.

Key words Motors, Nucleic-acid enzymes, RNA, Magnetic tweezers, Single molecule, Mechanochemistry

1 Introduction

Force has an essential role in a myriad of biological mechanisms. For example mechanical forces are generated in the cell during several processes like replication, transcription, translation, chromosomal segregation, and many others. Several techniques have been developed in the last 20 years with the capability to measure the forces and displacements generated by single molecules or to directly apply external forces to these processes in order to reveal their underlying molecular mechanisms. Single-molecule nano-manipulation techniques have made it possible to study protein activity under an applied mechanical stress. In fact, large structural rearrangements are often rate limiting, and applying assisting or opposing force can modulate these conformational changes and hence the catalytic cycle of molecular motors. The three commonly used single-molecule force-based manipulation methods are atomic force microscopy, optical tweezers, and magnetic tweezers. Here, we will describe the implementation of magnetic tweezers to directly measure the translocation activity of RNA motors.

Marc Boudvillain (ed.), *RNA Remodeling Proteins: Methods and Protocols*, Methods in Molecular Biology, vol. 1259, DOI 10.1007/978-1-4939-2214-7_16, © Springer Science+Business Media New York 2015

In a typical magnetic tweezers setup, a single nucleic-acid (NA) molecule is specifically tethered to a surface on one end and to a paramagnetic bead on the other (Fig. 1a). A pair of external permanent magnets generates a magnetic field that induces a magnetic moment on the bead that aligns with the lines of field (Fig. 1a). This induction leads to an external force that is proportional to the gradient of the scalar product between the induced magnetic moment and the magnetic field. This force is perpendicular to the field lines and points in the direction of the magnets (Fig. 1a). As the bead is tethered to the surface by single molecules, the magnetic force traps the bead in the axial direction [1, 2]. The force can be controlled by vertically translating the magnets in the axial direction and decreases exponentially with a typical decay constant of ~1 mm [2, 3]. Typical forces used in magnetic tweezers range from a few fN to ~10–20 pN [2], although larger forces can be attained (~100 pN). Several methods have been developed to estimate the trapping force by analysis of the Brownian motion of trapped beads [1, 3, 4].

In magnetic tweezers, the distance between the bead and the surface can be used as a direct, instantaneous measure of the NA tether length and employed to determine changes in NA extension due to protein activity (Fig. 1b). Importantly, the changes in NA tether extension (~few μm) are considerably smaller than the decay constant of the magnetic field (~1 mm), and therefore, the force on the paramagnetic bead can be considered constant and only defined by the distance between the magnets and the coverslip. The relation between extension of the tether and applied force depends on the mechanical properties of the NA molecule [5]. These mechanical properties vary considerably between single-stranded [6] and double-stranded DNA and RNA [7–10], and this difference was often used to monitor the conversion between single- and double-stranded NA molecules [11]. Importantly, magnetic tweezers allow for the application of torque by simply rotating the magnets [8] and the measurement of torque introduced by the activity of enzymes [12–15]. Critically, the ability of magnetic tweezers to apply torque on single double-stranded, topologically closed DNA molecules permits the introduction and control of the degree of supercoiling, making it the method of choice to investigate, for instance, the mechanisms of supercoiling regulation by DNA topoisomerases [16–19].

Fig. 1 (continued) extension of the NA tether is reduced (*right panel*). (**b**) The activity of RNA motors can lead to the change in the extension of the tether either by looping of the RNA substrate or by conversion from double- to single-stranded RNA (helicase activity). (**c**) The basic components of the illumination system and magnetic trap are shown: light from a fiber is first filtered by color to make it monochromatic, then collimated and guided to the sample by lenses L_1, L_2, and L_3 (see text). Magnets are positioned so that their axis is colinear with the optical axis of the objective and the illumination system. The position of the objective in the optical axis is controlled by a piezoelectric stage

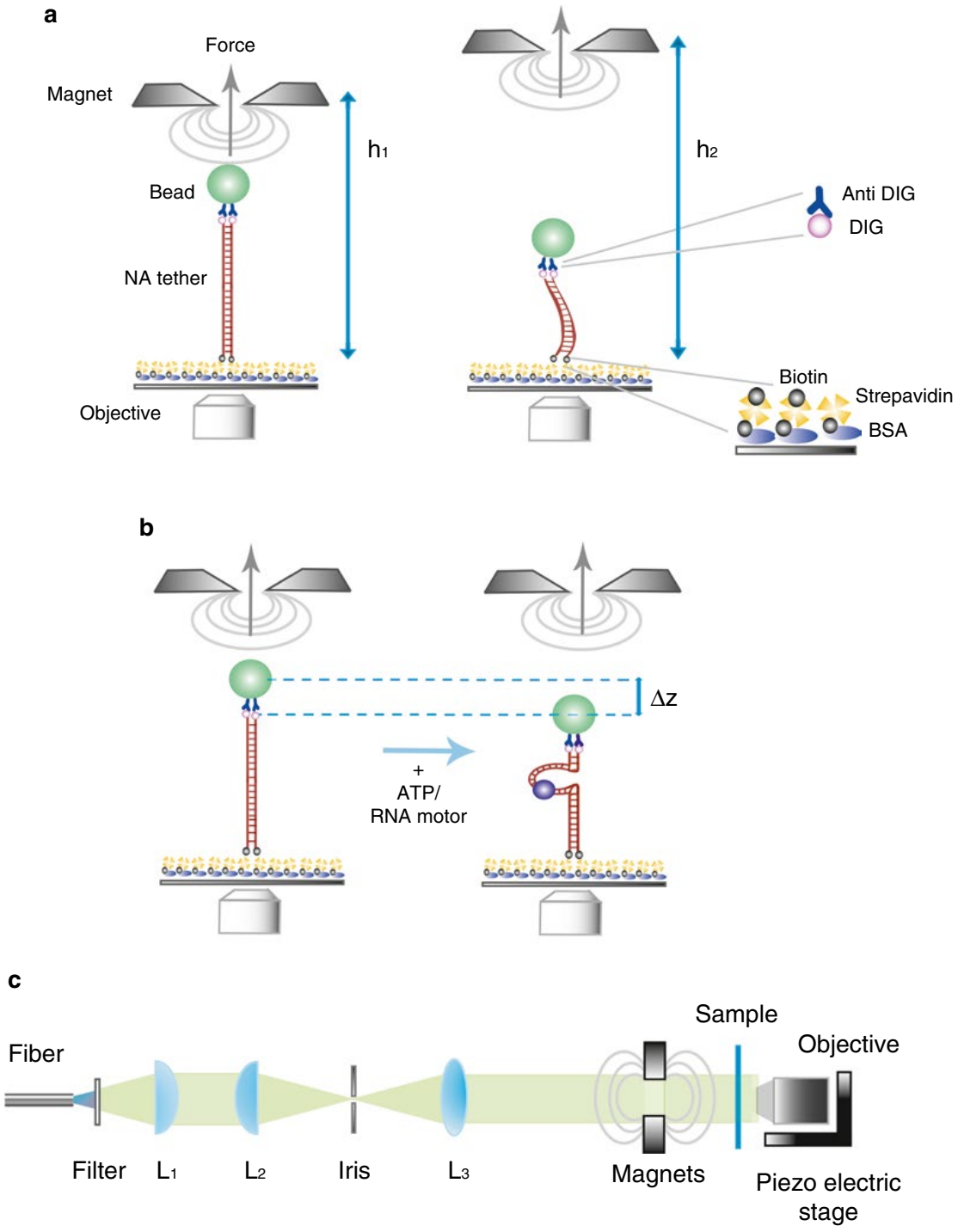

Fig. 1 Experimental design. (**a**) Schematic representation of a magnetic tweezers setup. A paramagnetic bead (*green sphere*) is attached to a single nucleic-acid (NA) molecule (*red vertical lines*) by DIG-anti-DIG interactions (*pink sphere* and *blue tripod*, respectively). On the other end, the NA tether is attached to the surface of the coverslip a flow cell by BSA-biotin/streptavidin/biotin linkages (*yellow trapezoids*, *gray sphere*, respectively). The presence of a pair of small magnets produces a magnetic field (*gray lines*) that produce a force on the bead proportional to the gradient of the field. The magnetic force exponentially decays with the distance between the magnets and the observation chamber (h). At higher distances, the force decreases and the

Magnetic tweezers are based on video microscopy and thus have an important advantage over other manipulation methods as multiple, single NA/bead attachments can be visualized at the same time. This advantage has been recently used to simultaneously monitor the trajectories of tens to hundreds of single molecules, considerably increasing the high throughputness of the method [20–22] and uniquely allowing for the detection of rare events at the single-molecule level [23].

The construction of a magnetic tweezers setup to study RNA helicases involves many hardware and software developments. Several methodological publications describe in detail the procedures used for the fabrication and use of microfluidics chambers for magnetic tweezers [24, 25], for the design and construction of DNA [25, 26] and RNA handles [10, 27], and for the characterization of forces [1, 3, 4]. In this chapter, we will concentrate on the construction of a simple magnetic trap and on the detailed description of the methodology used for image analysis.

Most algorithms used to determine the axial position of the magnetic bead rely on the interference ring pattern created by out-of-focus beads [28]. This interference pattern can be used to track beads in 3D with high precision. Several algorithms have been described in the literature that directly compare images of beads with simulated or real images of a library to obtain a vertical resolution of ~10 nm [2, 29–31]. Here, we will describe a considerably simpler method that does not rely on a comparison to a library of images, but rather on interpolating a signature of the interference ring that can be directly linked to the position of the bead in the vertical axis.

The methods section will begin by the construction of a simple magnetic trap, continue with a description of the image analysis methods used to extract the three-dimensional trajectory of magnetic beads (which translates into a measure of the extension of the NA tether), and end with a discussion of the steps involved in performing a typical magnetic tweezers experiment.

2 Materials

2.1 Illumination System

1. Fiber white light source (Thorlabs, OSL1-EC or OSL2). Lenses: L1 and L2 as aspheric lenses ($f = 17$ mm, MAP052525-A1), L3 is a spherical lens ($f = 10$ cm).
2. Translation stage (Thorlabs, PT1) mounted on a 1.5″ mounting post system (Thorlabs, P350/M, PB4/M, C1525, and PF175).
3. Cage components (30 mm diameter): four rods length 20 cm (Thorlabs, ER10) and material to mount cage to translation stage (Thorlabs, UPH6, TR3).
4. Bandpass filter (550–600 nm).

2.2 Microscope Components

1. An active optical table with vibration control (e.g., VH3660W-OPT table from Newport).
2. Commercial microscope with 1.4 numerical aperture, 100× oil objective, and at least one C-mount port.
3. CMOS (complementary metal oxide semiconductor) or CCD (charge-coupled device) camera (e.g., Neo and DU-885 cameras from Andor are good options for coupling with fluorescence applications). The camera has to be able to perform fast exposures (faster than 1 ms).
4. Closed-loop, high-resolution piezoelectric stage (MCL NanoF100).
5. Closed-loop motorized XY translation stage with rotary or linear encoders (ASI S31121010FT). The key feature in this component is the long-term stability, low lateral drift, and low degree of coupling between axes.
6. Digital to analog converter (NI USB-6211) (*see* **Note 1**).
7. Micrometer ruler slide (e.g., R1L3S2P from Thorlabs).

2.3 Magnet Mount

1. High-resolution linear translation stage (PI, M404.4PD) (*see* **Note 2**).
2. Fast rotation stage (typically >4 Hz) with high repeatability (PI, M-660.55) to permit the measurement of rapid, enzyme-induced changes in supercoiling levels and allow for accuracy in the angular positioning of the magnet axis.
3. 1.5″ mounting post system (Thorlabs, P350/M, PB4/M, C1525, and PF175) mounted on crossed, manual linear micrometric stages (Thorlabs, PT1) to align magnets on the optical axis.

2.4 Reagents and Small Equipment

1. Dynabeads MyOne carboxylic acid beads, 1 μm (Life Technologies) (*see* **Note 3**).
2. Phosphate buffer saline (PBS): 137 mM NaCl, 2.7 mM KCl, 10 mM Na_2HPO_4, and 1.8 mM KH_2PO_4.
3. Dynabeads MyOne streptavidin C1 beads (Life Technologies).
4. Streptavidin-coated magnetic beads 1 μm (Invitrogen).
5. Anti-digoxygenin (DIG) antibody.
6. Bovine serum albumin (BSA).
7. Biotinylated BSA solution: biotinylated BSA at 5 mg/ml in PBS. The solution is prepared from lyophilized biotinylated BSA by dilution into PBS (5 mg/ml), vigorous vortexing, and centrifugation. The solution is divided into 20 μl aliquots and stored at −20 °C.
8. 2 mg/ml streptavidin in PBS. Store at −20 °C as 30 μl aliquots.

9. 60 pmol/μl NA tether stock solution [10, 25–27] (see also chapter by Wei Cheng in this book).
10. Binding buffer: 50 mM Tris–HCl pH 7.5, 1 M NaCl, 1 mg/ml BSA.
11. Rotary incubator.

2.5 MicroFluidics

1. Home-made microfluidics chamber [24, 32]. Coverslips are typically washed with ethanol and dried before assembly of the microfluidics chamber. A detailed protocol for the preparation of microfluidic chamber is provided in the chapter by Wei Cheng in the present volume.

3 Methods

All steps below are performed at room temperature unless specified otherwise.

3.1 Construction of a Magnetic Trap

1. Assemble the illumination system as described in Fig. 1c. The first lens (L1) collimates the beam from the fiber light source, the second (L2) focuses it on the iris diaphragm, while the third lens (L3) is away from the iris by its focal length and collimates the beam into the flow chamber (Fig. 1c). Place the cage system vertically and align the fiber light source (*see* **Note 4**).
2. Magnets are centered on the optical axis of the objective (*see* **Note 5**).
3. Measure the pixel size of the camera by using a micrometer ruler slide. Typical pixel sizes are 80–100 nm.

3.2 Preparing Magnetic Beads and Generating NA-Bead Attachments

1. Assemble the microfluidics chamber and flush 1 ml of PBS through the channel.
2. Replace PBS in the channel with biotinylated BSA solution (s). Incubate for 2 h (*see* **Note 6**).
3. Flush out the BSA-biotin solution by passing 1 ml of PBS.
4. Prepare a fresh 0.2 mg/ml solution of streptavidin (*see* **Note 7**) and flush it into the channel. Incubate for 10 min.
5. Flush out streptavidin by passing 1–2 ml of PBS through the channel.
6. Transfer 0.5 μl of NA tether stock solution (60 pmol/μl) into a microtube and add 1 μl of a 1:10 dilution of anti-DIG beads (*see* **Note 3**). Add 1 μl of a dilution of streptavidin magnetic beads to the mix to be used as reference beads for drift correction. At the final concentration, streptavidin beads should be at a 1:10 molar ratio with respect to anti-DIG beads. Avoid pipetting this mix solution back and forth to limit NA shearing.

7. Add 3.5 μl of binding buffer and mix quickly by vigorous hand shaking. Avoid vortexing or centrifugation at all price, since these will shear the NA tether and precipitate beads.
8. Incubate solution in a rotary incubator for 10 min at room temperature. Then, add 45 μl of binding buffer.
9. Flush the solution into the channel of the microfluidic chamber while continuously imaging the coverslip surface on the CCD. Stop flow when beads appear on the field of view (FOV). After a short period, beads should start to fall on the coverslip surface.
10. After ~10–20 beads have set per FOV, turn the flow back on. The flow rate should be such that beads move on the surface at ~5 μm/s (*see* **Note 8**). Magnets should be far from the surface (>5–10 cm) during incubation; otherwise, beads will aggregate on the top surface of the channel.
11. After 10–20 min, approach the magnets to ~2–3 cm from the surface and explore different FOVs to detect proper bead attachments. A further description of this process can be found elsewhere [24].
12. Wash unattached beads until no more beads are seen to flow in the chamber. Only beads attached to the coverslip should be present. Nonspecifically attached beads can often be removed by manually passing a pair of fridge magnets close to the top surface of the microfluidics chamber.

3.3 Obtaining the Height of the Bead from Image Analysis

1. After illuminating the sample, image the interference pattern created by out-of-focus beads on a CCD camera. A typical FOV with several beads is shown in Fig. 2a. Beads are automatically segmented by following the procedure described in **steps 2–6**.
2. Subtract the minimum intensity of the image from all pixel intensity values and scale the resulting image so that its maximum intensity is unity.
3. Threshold the image to obtain a binary image. The threshold can be obtained by using the Otsu method, an algorithm that calculates the optimum threshold so that the combined intraclass variance between the two main intensity levels in the image is minimal. Perform a flood-fill operation on the background pixels to eliminate holes in the binary image.
4. Remove objects in the binary image with less than eight pixels (this parameter can be adjusted to improve results).
5. Classify objects in the binary image by finding the connected components.
6. Determine the centroids (x_i, y_i) and areas A_i of each object i. Keep only objects with large areas (usually >500 pixels).

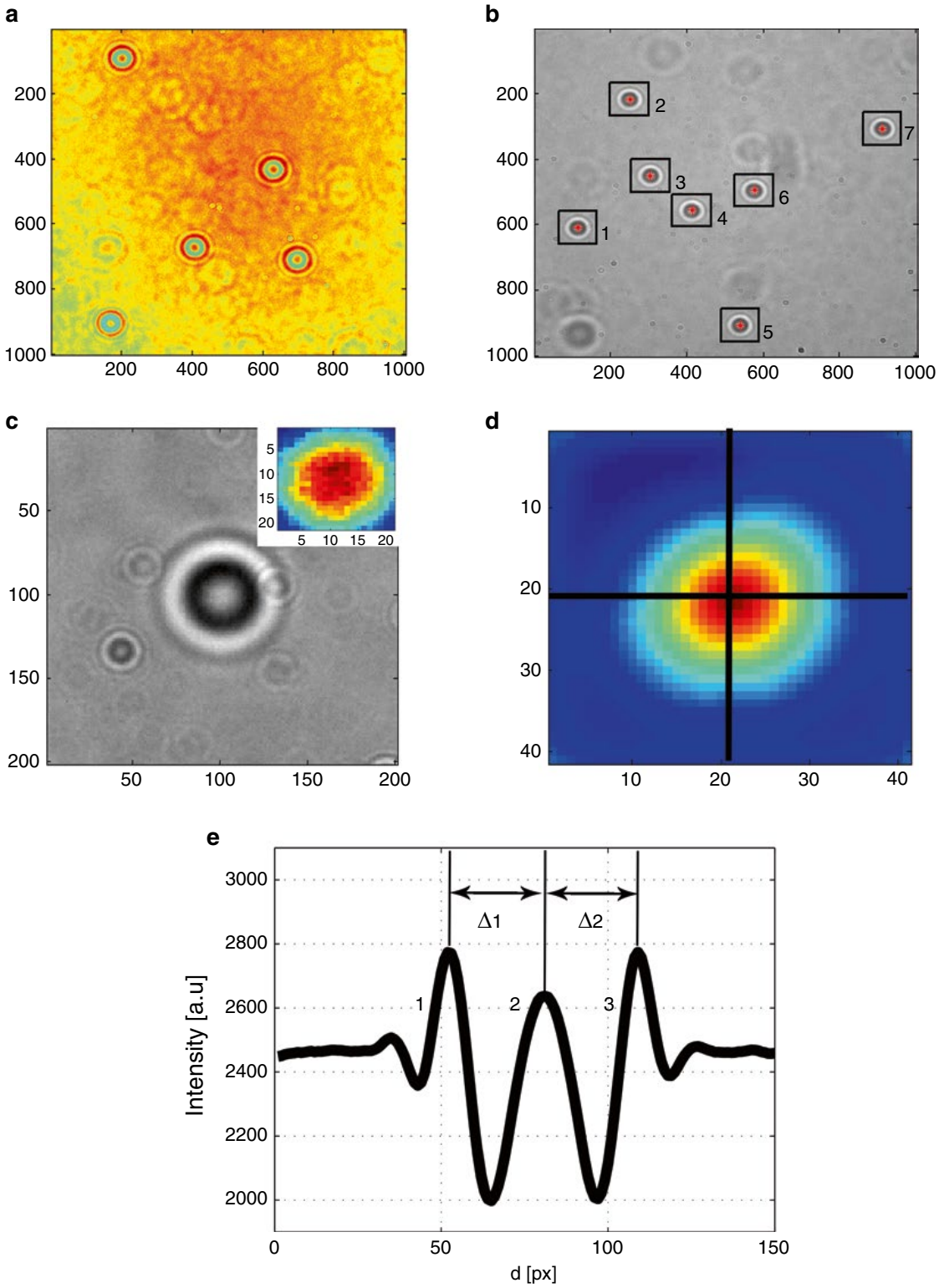

Fig. 2 Measurements of the bead axial position. (**a**) Interference patterns displayed by out-of-focus paramagnetic beads (1 μm) tethered to the surface by single NA attachments. Axes are in pixel units. (**b**) Bead segmentation is performed to automatically detect beads in the FOV. Boxes delimiting the ROIs used to extract the ring patterns of the beads (200 × 200 pixels) are shown as *black boxes*, while the position of the centers of the ROIs

The results of a typical segmentation are shown in Fig. 2b. Boxes around each bead represent the region of interest (ROI) occupied by that bead (usually 200×200 px, but this number depends on the total axial range to be calibrated and the density of beads in the FOV).

7. A typical ROI is shown in Fig. 2c (this image will be hereafter called I_1). The out-of-focus bead displays clear symmetric rings. Importantly, the distance between the rings and the center of the bead depends on the distance of the bead to the focal plane. This property is used to determine the axial position of beads. The first step in this procedure involves determining the centroid of the bead (center of symmetry). Our preferred method involves image cross-correlation and is described in **steps 8–11**.
8. Crop the image of the bead further by using a smaller ROI (usually 20×20 pixels). An example of the result of this operation is shown in the inset of Fig. 2c and will be hereafter called I_{ROI}.
9. Flip I_{ROI} in the horizontal and vertical directions to obtain $I_{ROI\text{-}flipped}$.
10. Determine the normalized cross-correlation between I_{ROI} and $I_{ROI\text{-}flipped}$ (I_{CC}) (see Fig. 2d for the cross-correlation function from the inset of Fig. 2c). Note that I_{CC} will have two times the vertical and horizontal dimensions of I_{ROI}.
11. Find the maximum of I_{CC} by determining the pixel with maximum intensity. First, determine the intensity profiles in the x and y directions at the center of the maximum. To interpolate the maximum of the I_{CC} function with sub-pixel resolution, perform a quadratic polynomial fit separately on each intensity profile and determine analytically the coordinates of the I_{CC} maximum from the coefficients of the polynomial series. Divide these coordinates by two to obtain the coordinates of the centroid of I_{ROI} with sub-pixel resolution. Convert, these coordinates into the coordinates of the image of the bead I_1 (Fig. 2c) by taking into account the different sizes of I_1 and I_{ROI}.
12. Determine the distance of the first concentric ring to the centroid of the bead as described in **steps 13–15**.

Fig. 2 (continued) are shown in *red*. Axes are in pixel units. (**c**) A typical ROI in which the interference rings can be clearly observed (bead 1 in panel **b**). Inset shows the cropped image (21×21 pixels) used for image cross-correlation (see text). Axes are in pixel units. (**d**) Image cross-correlation the inset in panel **c**. Crossed hairline indicates the center of the ROI. Coordinates of the bead centroid are calculated from the interpolated maximum of the cross-correlation image (see text). (**e**) Average intensity profile (ring pattern) of the intensity signal across the centroid of the bead (from image in panel **c**). Distances between peaks 1–2 and 2–3 define the values of Δ_1 and Δ_2

13. Using the coordinates of the centroid of the bead in image I_1 (**step 11**), plot the intensity profiles in the x and y directions across the centroid. The two intensity profiles are averaged to obtain the approximated ring profile of the bead (Fig. 2e, black thick line). Three maxima are clearly visible that correspond to the central bright spot of the bead and the first bright ring.
14. Determine the positions of the peaks with sub-pixel resolution by looking for downward zero crossings that exceed a certain threshold (usually set to zero).
15. Determine the distances Δ_1 and Δ_2 between the peaks corresponding to the centroid of the bead (peak 2 in Fig. 2e) and the first concentric ring (peaks 1 and 3). Average Δ_1 and Δ_2 to obtain Δ (pixel units). Δ is a parameter that shows a one-to-one correspondence to the axial distance between the bead and the focal plane (*see* **Note 9**).

Other algorithms exist that obtain a parameter from the image that is strictly related to the vertical position of the bead. These algorithms use the Hilbert transform to calculate the phase shift between ring patterns [2] or calculate the entropy of the image without even needing to obtain a precise estimation of the centroid of the bead. In our hands, the algorithm described here is the fastest and displays excellent vertical resolution (~1.4 nm in a 1 s window; see Fig. 3d).

3.4 Determining and Applying a Calibration

1. To determine the relation between Δ and the distance of the bead to the objective focal plane (calibration function), take images of the bead at different focal positions of the objective using the piezoelectric stage holding the objective (usually steps of 50 nm are taken) (*see* **Note 10**). The ring profile dramatically changes with the position of the objective (defined as z) (Fig. 3a). In the example shown, six positions were acquired with a step size of 500 nm.
2. Plot the value of Δ for each profile i (Δ_i) against z_i (Fig. 3b). Use a second-order polynomial ($z(\Delta) = A_0 + A_1\,\Delta + A_2\,\Delta^2$) to interpolate Δ for any value of z in the scanned interval (solid line in Fig. 3b).
3. Test the calibration by first acquiring a dataset in which the whole z range is scanned. In a test example, we obtained ten images for each z position, with a step size of 500 nm. The resulting images were analyzed as described in Subheading 3.3 and Δ was obtained for each frame. Δ was then converted into height by using the polynomial interpolation $z(\Delta)$ (**step 2**). The obtained z positions were plotted against frame number to verify that the distance between steps corresponds to the step size used in the acquisition (Fig. 3c).

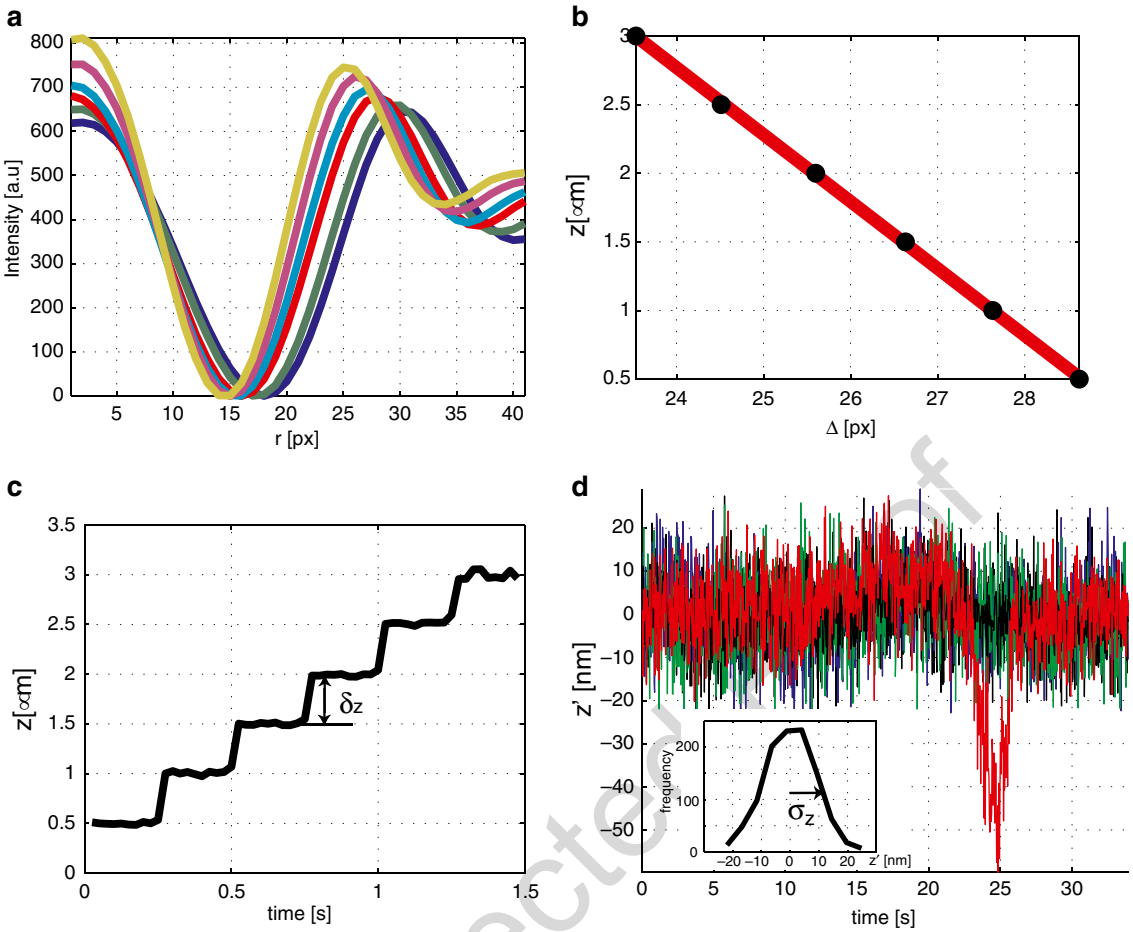

Fig. 3 Application of the bead calibration. (**a**) Variation of the ring pattern with position of the focal plane. The change in phase of the rings is approximately proportional to the distance of beads to the focal plane. (**b**) Plot of the focal position (z) as a function of Δ (*black open circles*). *Solid line* represents a second-order polynomial fit to the experimental data. (**c**) The calibration is tested by running a mock experiment in which the focal position of the objective is shifted in steps of $\delta z = 500$ nm (10 images per position). (**d**) Single-molecule time traces of the vertical position of four tethered beads in the same FOV (z'). Most tethers do not show activity (*black*, *blue*, and *green*) and their vertical position fluctuates due to Brownian motion. In contrast, the red trace shows a typical single-molecule ssRNA looping event. Inset shows the frequency of z' positions for a single-tethered bead displaying Brownian motion. σ_z represents the standard deviation of the distribution (10 nm at 40 Hz)

For an FOV with multiple beads, calibration parameters are obtained for each bead and used to analyze the distance changes of each bead during an experiment. To perform this process in tethered beads, high forces (~10 pN) are used to limit axial movement during the acquisition of the calibration file.

3.5 Performing an Experiment and Analyzing Data

1. After assembling the microfluidics chamber and obtaining tethered beads (procedure extensively described elsewhere [24]), characterize the length of each attached bead in the FOV, using the buffer in which experiments will be performed.

The most common procedure involves measuring the tether extension as a function of force and performing a fit to a worm-like chain model. This procedure provides the persistence length of the NA tether and its full extension. Use only beads displaying correct full extension and persistence length for experiments.

2. After tether characterization, introduce a solution containing the protein under study into the chamber (*see* **Note 11**).
3. Any protein activity that changes the length of the NA tether (like a looping enzyme that shortens the extension of the tether, or a helicase converting the NA construct from double-stranded to single-stranded form) will generate a change in the vertical position of the bead. The change in axial position of each bead in the FOV is measured by determining Δ for each bead and each image and by using the bead-specific calibration function to obtain a z position. This calculation can be performed in off-line mode (by registering a movie of the FOV over long time periods and performing post-analysis, *see* **Note 12**) or in real time (by image analysis performed on-the-fly, *see* **Note 13**).
4. Correct z-axis values for the displacement of the objective. The displacement of the objective does not correspond to that of the focal plane due to refraction of light at the water-glass interface. The real axial position of the bead (z') is obtained by $z' = z\ n_{\text{water}}/n_{\text{glass}} \sim 0.86\ z$, where n_{water} and n_{glass} are the indexes of refraction of water and glass and z is the axial position calculated by moving the piezoelectric stage.
5. Correct the extension over time for each bead, $z'_i(t)$, to account for axial drift (*see* **Note 14**). This procedure is performed by following in parallel the z position of a bead that is stuck to the surface ($z'_{\text{stuck}}(t)$; *see* **Note 15**) and by subtracting the average axial position of the stuck bead from the positions of all beads (*see* **Note 16**). In other words, drift corrected extensions are obtained by $z'_{i,\text{corrected}}(t) = z'_i(t) - \langle z'_{\text{stuck}}(t) \rangle$. An example of the tracking of several beads after drift subtraction is shown in Fig. 3d.
6. Scan the traces of each bead in the FOV manually or automatically to detect single-molecule events (*see* **Note 17**). A typical looping event is shown in Fig. 3d. These events can be used to obtain information on the processivity, the velocity, and the pause length behavior of the enzymatic reaction at the single-molecule level.

4 Notes

1. A DAQ is essential for performing the z-axis calibration by triggering the camera exposure at the same time as the piezoelectric stage is moved. If communication with the piezoelectric stage is through an analog signal, the card should have

enough bits (usually 16 bits is recommended) to encode small enough changes in the position of the stage.

2. This translation stage should be fast (>10 mm/s) and precise (usually ~1–2 μm) to allow for rapid and small changes in force, show a low-pitch yaw angle (~50 μrad) to avoid lateral displacement during a long vertical translation, display high repeatability (typically ~1–2 μm) to ensure repeatable forces are attained during an experiment, and accept high loads (>100 N) in vertical configuration to allow for the displacement of magnets and the rotation stage.
3. MyOne beads are functionalized with anti-DIG antibodies by following the standard protocol of the vendor. 300 mg of antibody are used per derivatization procedure. Derivatized beads can be kept at 4 °C for years. Beads will precipitate to the bottom of the tube and form large aggregates. Before use, the stock is vortexed and 2 μl of bead slurry are taken to make a 1:10 dilution of the stock in a 0.5 ml microtube using PBS buffer (final volume 20 μl). This dilution is sonicated by placing the microtube in a glass container filled with water and by approaching the microtube to a tip sonicator (for a total time of ~5′). This same 1:10 solution can be used two to three times (sonication tends to shear beads and so it is not desirable to sonicate the same bead solution many times).
4. It is important that the lamp is placed on a shelf and not in contact with the optical table to avoid the transmission of vibrations to the microscope.
5. Magnet alignment is achieved by positioning the magnets close to the objective lens and imaging the resulting transmitted light pattern on the camera. The magnets act as an iris that blocks the light transmitted to the objective. Their alignment on the optical axis is performed by maximizing the symmetry and homogeneity of the transmitted light pattern on the camera by displacing the micrometer manual translation stages used to mount the magnets. Then, the magnets are displaced vertically, and the process is repeated to ensure that the axis of translation of the vertical translation stage holding the magnet is colinear to the optical axis. Once tethers are obtained, a finer alignment is made by rotating the magnets while simultaneously tracking the centroid of tethered beads. Misaligned magnets lead to non-vertical forces and to elliptical orbits of the tracked bead during magnet rotation [33].
6. For each channel, a new tube of biotinylated BSA is thawed and used only once. By inserting air before and after the arrival of BSA-biotin into the channel, the use of this relatively expensive reagent can be minimized, and the arrival of the BSA-biotin solution can be directly observed. Tubes are clamped

during the incubation to avoid water evaporation and drying of the channel.

7. For each experiment, an aliquot of streptavidin stock is thawed and a 1:10 dilution is made with PBS to a final volume of 50 μl. The dilution can be kept at 4 °C for no more than 1 week (do not refreeze).
8. If the flow rate is too high, beads will not remain in contact to the surface and attached beads may nonspecifically bind to the surface. If flow is too slow, beads risk on bouncing on each other to form large aggregates.
9. The determination of bead height by using Δ is robust, as (1) Δ is independent on intensity, and (2) the fact that the relative distance of the first peaks to the center are used (and not the real position of the center) means that errors in the centroid determination show a lower degree of coupling into the height determination than with other methods that rely on the absolute ring pattern.
10. Calibration curves are obtained for each tethered bead. To ensure that the beads move as little as possible in the axis due to Brownian motion during the acquisition, the force exerted by the magnet is set to its maximum (usually ~10 pN). In addition, the exposure time of the camera is reduced as much as possible to limit image blurring (typical 2–5 ms).
11. The enzyme is prepared at a low enough concentration to ensure single-molecule conditions (typical concentrations are 1–10 nM, but depend on the affinity of NA association constant of the enzyme and on its oligomerization constant). Typically, the buffer used is the same as that providing strong "in bulk" activity, but usually contains BSA to avoid nonspecific interactions. Often, enzymes show the tendency of interacting nonspecifically with the tubes and glass in the chamber (even if these are passivated by BSA). This effect can be more deleterious at low enzyme concentration as, in this case, most of the protein may end up in the tubes and not in the NA substrate. In such cases, a low concentration of a detergent (i.e., Tween-20) or a higher concentration of BSA (0.1 mg/ml final) can be used. Protein is usually kept on ice before injection into the chamber to maintain its enzymatic activity.
12. For off-line acquisition and analysis, movies are acquired in frame transfer mode, with a 25 ms exposure time for as long as 30 min. Data are stored in spooling mode on a solid-state drive (SSD) to improve writing and reading speeds (the latter is very important for image analysis of long movies). The SSD disk is emptied before each experiment as writing large files in spooling mode in fragmented drives often leads to incomplete movies or movies with empty frames. Movies are saved as

uncompressed TIFF files to avoid data loss during compression. Image analysis in MATLAB is performed on the movies to track beads in 3D and analyze trajectories.

13. Real-time acquisition is paramount when the user needs to react to the activity of the enzyme. Typical example is the study of topoisomerases, in which supercoiling needs to be introduced to generate the substrate on which the enzyme reacts (see for example [19]). After a processive reaction cycle of the enzyme, a new substrate needs to be generated by the user, making a real-time analysis tool almost unavoidable. A second case in which real time is essential arrives when the activity of the enzyme destroys the substrate, as is the case for DNA translocases that can irreversibly pull DNA to the surface unless sufficient force is exerted on the bead. As the initiation rate of the translocation activity is strongly force dependent, a real-time feedback on the current activity of the motor protein is required (see for instance [34]). We implemented real-time acquisition and analysis in LabVIEW with analysis routines implemented as external C libraries.
14. Typical magnetic tweezers experiments rely on following the extension of tethered beads for extended periods of time (10 min to hours). During these long periods, thermal expansion or contraction of the different components of the microscope due to temperature changes in the environment produces slow changes in the distance between the objective and the chamber (drift). This drift can be minimized by properly choosing the components used in the microscope, assuring a constant temperature in the room and of all components used (such as the buffer injected into the microfluidics chamber), but it is ultimately impossible to eliminate it completely.
15. In FOV with many beads, it is common to find beads attached nonspecifically to the surface that can serve as stuck beads for drift subtraction. Alternatively, the bead-NA mix can be supplemented with a low concentration of streptavidin beads that will specifically fix to the surface. A third possibility is to fuse polystyrene beads to the surface by depositing them and heating them on the coverslip before assembly of the microfluidics chamber.
16. The drift of the chamber during acquisition can be obtained by following the axial movement of a stuck bead $z'_{\text{stuck}}(t)$ and filtering the signal by using a mean-filter function that averages the signal on a defined time window (typically ~1 s) to obtain $\langle z'_{\text{stuck}}(t)\rangle$. The drift in all beads can be corrected by subtracting $\langle z'_{\text{stuck}}(t)\rangle$ from the trajectories of each bead. Alternatively, if no stuck bead is present, and there are several (>5) beads in the FOV, an alternative approach consists in averaging the axial coordinates of all beads in the FOV to obtain the mean drift. Care must be taken to eliminate beads from this average that

display single-molecule events due to enzymatic activity. A second approach to eliminate drift has been recently developed that uses the Allan variance [4].

17. Single-molecule conditions are statistically achieved when the time between events (t_2) is considerably larger than the typical duration of a single event (t_1). The probability of two events occurring at the same time by chance is $(t_1/t_2)^2$. Thus, if $t_1/t_2 = 0.05$, the probability of two single-molecule events overlapping becomes <1 %.

Acknowledgments

We thank Francesco Pedaci and Antoine Le Gall for critical reading and very helpful comments. Financial support was provided by the Human Frontiers Science Program (M.N.) and the European Research Council (Starting Grant 260787 to M.N.).

References

1. te Velthuis AJW, Kerssemakers JWJ, Lipfert J et al (2010) Quantitative Guidelines for Force Calibration through Spectral Analysis of Magnetic Tweezers Data. Biophys J 99: 1292–1302
2. Lionnet T, Allemand JF, Revyakin A et al (2012) Single-molecule studies using magnetic traps. Cold Spring Harb Protoc 2012:34–49
3. Vilfan ID, Lipfert J, Koster DA et al (2009) Magnetic Tweezers for Single-Molecule Experiments, Handbook of Single-Molecule Biophysics. Springer, New York
4. Lansdorp BM, Saleh OA (2012) Power spectrum and Allan variance methods for calibrating single-molecule video-tracking instruments. Rev Sci Instrum 83:025115
5. Strick T, Allemand J, Croquette V et al (2000) Twisting and stretching single DNA molecules. Prog Biophys Mol Biol 74:115–140
6. Smith SB, Cui Y, Bustamante C (1996) Overstretching B-DNA: the elastic response of individual double-stranded and single-stranded DNA molecules. Science 271:795–799
7. Bustamante C, Marko JF, Siggia ED et al (1994) Entropic elasticity of lambda-phage DNA. Science 265:1599–1600
8. Strick TR, Allemand JF, Bensimon D et al (1996) The elasticity of a single supercoiled DNA molecule. Science 271:1835–1837
9. Herrero-Galán E, Fuentes-Perez ME, Carrasco C et al (2013) Mechanical identities of RNA and DNA double helices unveiled at the single-molecule level. J Am Chem Soc 135:122–131
10. Abels JA, Moreno-Herrero F, van der Heijden T et al (2005) Single-molecule measurements of the persistence length of double-stranded RNA. Biophys J 88:2737–2744
11. Liphardt J, Onoa B, Smith SB et al (2001) Reversible unfolding of single RNA molecules by mechanical force. Science 292:733–737
12. Lipfert J, Wiggin M, Kerssemakers JWJ et al (2011) Freely orbiting magnetic tweezers to directly monitor changes in the twist of nucleic acids. Nat Commun 2:439
13. Lebel P, Basu A, Oberstrass FC et al (2014) Gold rotor bead tracking for high-speed measurements of DNA twist, torque and extension. Nat Methods 11:456–462
14. Bryant Z, Oberstrass FC, Basu A (2012) Recent developments in single-molecule DNA mechanics. Curr Opin Struct Biol 22:304–312
15. Mosconi F, Allemand JF, Bensimon D et al (2009) Measurement of the torque on a single stretched and twisted DNA using magnetic tweezers. Phys Rev Lett 102:078301
16. Crisona NJ, Strick TR, Bensimon D et al (2000) Preferential relaxation of positively supercoiled DNA by E. coli topoisomerase IV in single-molecule and ensemble measurements. Genes Dev 14:2881–2892
17. Stone MD, Bryant Z, Crisona NJ et al (2003) Chirality sensing by Escherichia coli topoisomerase IV and the mechanism of type II topoisomerases. Proc Natl Acad Sci U S A 100:8654–8659
18. Koster DA, Croquette V, Dekker C et al (2005) Friction and torque govern the relaxation of

DNA supercoils by eukaryotic topoisomerase IB. Nature 434:671–674

19. Nollmann M, Stone MD, Bryant Z et al (2007) Multiple modes of Escherichia coli DNA gyrase activity revealed by force and torque. Nat Struct Mol Biol 14:264–271
20. Ribeck N, Saleh OA (2008) Multiplexed single-molecule measurements with magnetic tweezers. Rev Sci Instrum 79:094301
21. De Vlaminck I, Henighan T, van Loenhout MTJ et al (2011) Highly Parallel Magnetic Tweezers by Targeted DNA Tethering. Nano Lett 11:5489–5493
22. Ding F, Manosas M, Spiering MM et al (2012) Single-molecule mechanical identification and sequencing. Nat Methods 9:367–372
23. Manosas M, Perumal SK, Croquette V et al (2012) Direct observation of stalled fork restart via fork regression in the T4 replication system. Science 338:1217–1220
24. Manosas M, Meglio A, Spiering MM et al (2010) Magnetic Tweezers for the Study of DNA Tracking Motors. Methods Enzymol 475:297–320
25. Lionnet T, Allemand JF, Revyakin A et al. (2011) Magnetic trap construction. Cold Spring Harb Protoc 2012, pdb.prot067496–pdb.prot067496
26. Revyakin A, Ebright RH, Strick TR (2005) Single-molecule DNA nanomanipulation: improved resolution through use of shorter DNA fragments. Nat Methods 2:127–138
27. Cheng W, Dumont S, Tinoco I et al (2007) NS3 helicase actively separates RNA strands and senses sequence barriers ahead of the opening fork. Proc Natl Acad Sci U S A 104:13954–13959
28. Ovryn B, Izen S (2000) Imaging of transparent spheres through a planar interface using a high-numerical-aperture optical microscope. J Opt Soc Am A Opt Image Sci Vis 17:1202–1213
29. Gosse C, Croquette V (2002) Magnetic tweezers: micromanipulation and force measurement at the molecular level. Biophys J 82:3314–3329
30. van Loenhout MTJ, Kerssemakers JWJ, De Vlaminck I et al (2012) Non-Bias-Limited Tracking of Spherical Particles, Enabling NanometerResolution at Low Magnification. Biophys J 102:2362–2371
31. Lipfert J, Kerssemakers JJW, Rojer M et al (2011) A method to track rotational motion for use in single-molecule biophysics. Rev Sci Instrum 82:103707
32. Cattoni DI, Fiche J-B, Valeri A et al (2013) Super-resolution imaging of bacteria in a microfluidics device. PLoS One 8:e76268
33. De Vlaminck I, Henighan T, van Loenhout MTJ et al (2012) Magnetic Forces and DNA Mechanics in Multiplexed Magnetic Tweezers. PLoS One 7:e41432
34. Ptacin JL, Nollmann M, Becker EC et al (2008) Sequence-directed DNA export guides chromosome translocation during sporulation in Bacillus subtilis. Nat Struct Mol Biol 15:485–493